

Ilex paraguariensis Extract-Coated Magnetite Nanoparticles: A Sustainable Nano-adsorbent and Antioxidant

**D. Fabio Mercado, Paula Caregnato,
Laura S. Villata & Mónica C. Gonzalez**

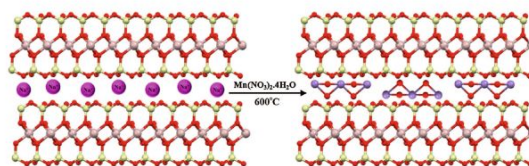
**Journal of Inorganic and
Organometallic Polymers and
Materials**

ISSN 1574-1443

J Inorg Organomet Polym
DOI 10.1007/s10904-017-0757-8



JOURNAL OF
INORGANIC AND
ORGANOMETALLIC
POLYMERS AND
MATERIALS



 Springer

Volume 27, Number 1
JANUARY 2017

27(1) 1–384 (2017)
ISSN 1574-1443

 Springer

Your article is protected by copyright and all rights are held exclusively by Springer Science+Business Media, LLC, part of Springer Nature. This e-offprint is for personal use only and shall not be self-archived in electronic repositories. If you wish to self-archive your article, please use the accepted manuscript version for posting on your own website. You may further deposit the accepted manuscript version in any repository, provided it is only made publicly available 12 months after official publication or later and provided acknowledgement is given to the original source of publication and a link is inserted to the published article on Springer's website. The link must be accompanied by the following text: "The final publication is available at link.springer.com".



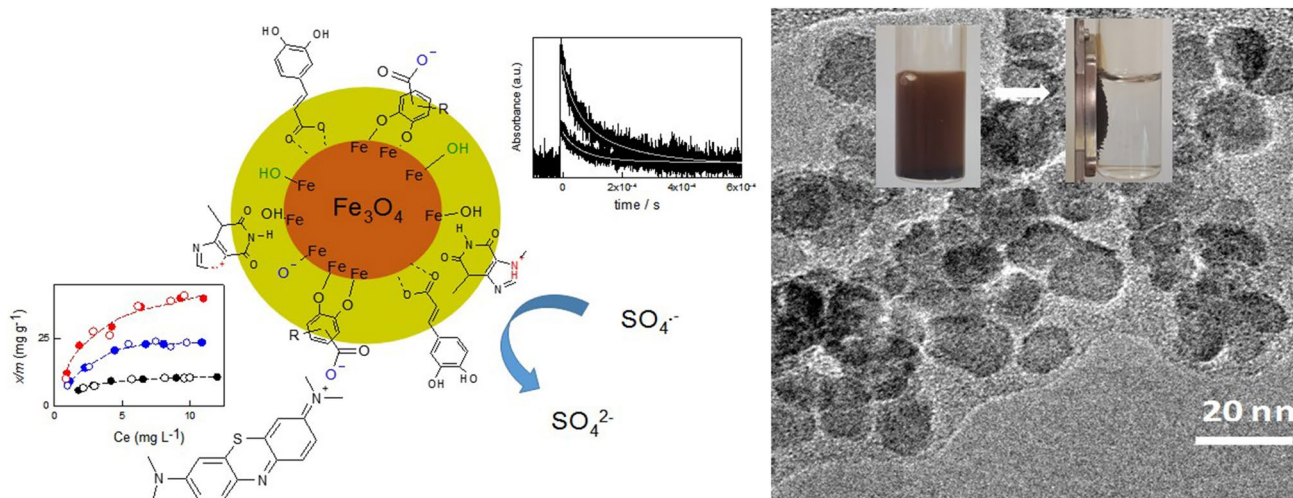
Ilex paraguariensis Extract-Coated Magnetite Nanoparticles: A Sustainable Nano-adsorbent and Antioxidant

D. Fabio Mercado¹ · Paula Caregnato¹ · Laura S. Villata¹ · Mónica C. Gonzalez¹Received: 15 September 2017 / Accepted: 27 November 2017
© Springer Science+Business Media, LLC, part of Springer Nature 2017

Abstract

Single-crystal 15 nm size magnetite nanoparticles were synthesized and coated with Yerba Mate (*Ilex paraguariensis*) extract to evaluate their use as versatile antioxidant magnetic nanoadsorbents. The obtained particles, Mnp@YM, were found to be composed of a crystalline magnetite core surrounded by a shell composed of Fe₃O₄, FeO, and Fe₂O₃ oxides. YM extract resulted an effective protective coating for Mnp incorporating surface carboxylates, phenols, and organic N groups which improve the particles stability in aqueous suspensions. Mnp@YM antioxidant capacity (1.8 μM Trolox equivalent per 0.1 mg YM coating contained in 1 mg L⁻¹ particle suspension) is of the order reported for polyphenols. SO₄^{•-} scavenging rate constant (1.5 × 10⁴ g⁻¹ L s⁻¹) is within the diffusion controlled regime for 15 nm spherical nanoparticles with homogeneously distributed reactive sites. Mnp@YM reversibly adsorbs MB with maximum adsorption of 50 mg g⁻¹. As a consequence of these capacities, Mnp@YM resulted effective in preventing MB oxidation by peroxodisulfate.

Graphical Abstract

**Keywords** Radical scavenger · Sulfate radicals · ABTS^{•+} · Nanoadsorbent · Methylene blue

Electronic supplementary material The online version of this article (<https://doi.org/10.1007/s10904-017-0757-8>) contains supplementary material, which is available to authorized users.

✉ Mónica C. Gonzalez
gonzalez@inifta.unlp.edu.ar

Extended author information available on the last page of the article

1 Introduction

Due to their magnetic properties, size, shape, and biocompatibility, magnetite nanoparticles, Mnp, have attracted growing interest in several areas spanning from biological and medical applications to environmental remediation [38]. Mnp are susceptible to air and water oxidation [35] leading to the

formation of a mechanically unstable and chemically active outer layer composed of Fe_2O_3 and $\text{FeO}(\text{OH})$ [12]. Thus, stabilization by surface coating is an important issue in applications development of Mnp. In particular, adsorption of natural polymers [13], humic acid [20, 45] and bioorganic wastes [23] showed Mnp enhanced stability and improved capability as adsorbent of metal ions and organic trace pollutants.

Ilex paraguariensis, familiarly known as Yerba Mate (YM), is an interesting coating natural material to expand Mnp applications. YM represents an important economic activity in several South American countries as YM leaf extracts are intensively consumed as infusions and used in the formulation of foods. High concentrations of tannins, saponins, methylxanthines, and flavonoids provide a significant amount of phytochemical compounds to the herb [18] while the high content of bioactive polyphenolic compounds as caffeic, quinic, caffeoylquinic, feruloylquinic, and dicaffeoylquinic acids, quercetin and rutin are responsible for YM antioxidant properties [5, 7].

Antioxidants counteract oxidation processes by several mechanisms as free radicals and molecular singlet oxygen scavenging and chelation of metal ions capable of accelerating oxidation. Incorporation of natural antioxidants in magnetic matrices is of technological interest as they could be easily removed by application of a magnetic field thus overcoming oxidation and polymerization drawbacks in the long-term [11]. Among the magnetic supports used, mainly FeO nanoparticles synthesized using *Amaranthus spinosus* leaf extracts were reported to show abilities as antioxidants and as photocatalysts [27].

In this study, we report the preparation and characterization of YM extract-coated magnetite nanoparticles in an attempt to design a novel magnetic nanoparticle with an active adsorbing surface and efficient antioxidant activity. The nanoparticles radical scavenging capacity was evaluated using both, the stable 2,2'-azino-bis-3-ethylbenzthiazoline-6-sulphonic acid ($\text{ABTS}^{+\bullet}$) radical standard and the highly reactive $\text{SO}_4^{\cdot-}$ radical anion ($\epsilon^0 = 2.6 \text{ V}$). Adsorption capabilities were evaluated using the cationic dye methylene blue (MB) as a probe.

MB in low doses has many safe uses in medicine and biology [15]. However, its extensive use in industrial processes leads to colored and contaminated discharge effluents. Removal of MB from wastewater by low-cost adsorbents is regarded as superior to other techniques when water re-use is required [Rafatullah et al. 30].

2 Materials and Methods

Reactants and standard equipment and methods used for characterization purposes [FTIR, IR-ATR, XRD, HRTEM, TGA, DLS, UV-Vis, Raman, and Zero Point pH (pH_{PZC})] are described in the Online Resource pages 2–5.

2.1 Synthesis of YM-Coated Magnetite Nanoparticles

Briefly, 6.1 g of $\text{FeCl}_3 \cdot 6\text{H}_2\text{O}$ and 4.2 g of $\text{FeSO}_4 \cdot 7\text{H}_2\text{O}$ were dissolved in 100 mL of ultrapure H_2O under continuous stirring and heating to 90 °C. Magnetite was coprecipitated by the addition of 10 mL of a 25% ammonium hydroxide solution, followed by the addition of 50 mL YM extract to obtain a suspension of YM-coated magnetite nanoparticles. The suspension was maintained under constant heating and stirring for ca. 30 min. The precipitate was separated from the mother liquor by application of a magnetic field from a laboratory magnet bar of ca. 2500 GS, washed several times with deionized water, dried at 70 °C under vacuum, and stored in dark-colored flasks. For the preparation of magnetite nanoparticles with no coating (Mnp), the same procedure was applied except that the 50 mL YM extract was replaced by pure water.

YM extracts were prepared upon addition of 1 L of ultrapure water to 10 g YM and left in contact under continuous stirring for 1 h at 70 °C. To obtain different coating coverage, the YM extract was either used “as obtained” or 40% diluted with ultra-pure water. The solids thus synthesized are named Mnp@YM10 and Mnp@YM4, respectively. As will be discussed later, the number in the particles name stands for the % w/w of YM extract per g particle.

2.2 Experimental Methods

$\text{ABTS}^{+\bullet}$ scavenging experiments were performed by an Spectrophotometric Assay [42] described in Online Resource pages 6–7. $\text{SO}_4^{\cdot-}$ radical anion scavenging experiments were performed by time-resolved Laser Flash Photolysis experiments (LFP) described in the Online Resource page 8.

Adsorption studies were conducted in batch experiments at 25 ± 2 °C as described in Online Resource page 9. Adsorption isotherms were obtained plotting the weight in mg of adsorbed MB per g particles, x/m (mg g^{-1}), versus MB solution equilibrium concentration, C_e (mg L^{-1}).

Experiments on the protecting effect of Mnp@YM10 against MB oxidation by peroxodisulfate in aqueous solutions were conducted at 25 ± 2 °C. Experimental details are described in the Online Resource page 10.

3 Results and Discussion

3.1 Particle Characterization

HRTEM micrographs of Mnp and Mnp@YM10, see Online Resource page 11, clearly depict the individual irregular round-shaped magnetite nanoparticles. The 15 ± 1 nm size crystalline particles show plane spacing of *ca.* 2.5 Å, in line with those of d311 planes of magnetite. Mnp and Mnp@YM10 saturation magnetization at 300 K are of 59.0 and 55.4 emu/g [25], respectively, in line with reported values for similar sized magnetite nanoparticles [9]. The observed magnetic properties allowed the easy extraction of the particles from suspension by application of a magnetic field from a laboratory magnet, as shown in the Graphical Abstract.

XRD diffractograms of all the particles (see Online Resource page 12) show diffraction peaks at $2\theta = 30.4, 35.5, 43.5, 53.8, 57.2,$ and 63.0 characteristic of magnetite (Powder Diffraction file, JCPDS no. 85-1436). Mnp and Mnp@YM10 crystallite domain sizes of 15 and 12 nm, respectively, are estimated employing Scherrer equation and considering peak broadening at $2\theta = 35.5$, a shape factor of 0.9, and 0.154056 nm as the wavelength for Cu K α 1 X-ray radiation. The coincidence between the crystallite size obtained by XRD and the nanoparticle Feret diameter observed by HRTEM suggest a single crystal particle.

The FTIR spectrum of Mnp, see Fig. 1 inset, shows adsorption peaks at 555 and 640 cm^{-1} characteristic of Fe–O stretching as well as broad bands in the 1640 and 3440 cm^{-1} regions due to $\delta\text{H–O–H}$ and νOH vibrations of lattice and physisorbed water molecules. Mnp also shows a small band at 1460 cm^{-1} attributed to adsorbed carbonate. Aside from

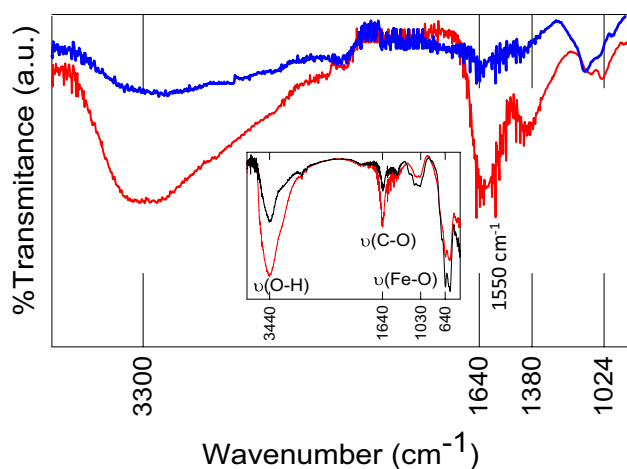


Fig. 1 ATR-FTIR spectra of Mnp@YM4 (blue lines) and Mnp@YM10 (red lines). Inset FTIR spectra of Mnp (black lines) and Mnp@YM10 (red lines). (Color figure online)

the characteristic Fe–O bands, the spectrum of Mnp@YM10 evidences bands at 3440 and 1640 cm^{-1} also observed for Mnp. However, the intensity ratios of these bands with respect to that of FeO (I_{3440}/I_{555} and I_{1640}/I_{555} , respectively) are between 3 and 2.6 times bigger for Mnp@YM10 than for Mnp. Thus, the contribution of YM components to the 3440 and 1640 cm^{-1} bands in the FTIR spectrum of Mnp@YM10 is supported. The intense asymmetric broad band with maximum absorption around 3440 cm^{-1} may be attributed to HO while N–H groups may contribute near 3200 cm^{-1} . The 1640 cm^{-1} broad band may be attributed to carbonyl stretching as in xanthenes [17] and in carboxylate-metal monodentated complexes [16].

The FTIR-ATR spectrum (see Fig. 1) being mainly sensitive to surface molecules, show the already described bands centered at 3440–3200 and 1640 cm^{-1} and more defined bands at *ca.* 1550 and 1380, attributed to free carboxylates in hydroxybenzoic acids and in bidentate metal complexes, respectively [16, 44]. However, plant polyphenols were also reported to show phenolic HO vibrations around 1385 cm^{-1} [40]. Bands at 1100 and 1025 cm^{-1} are characteristic of catecholate complexes with transition metals [4] and aromatic C–C, and of C–O single bond stretching, respectively. The intensity of these bands increase with the YM coverage. Altogether, IR data supports the formation of chelate structures between carboxyl and phenolic groups of YM components and surface Fe ions on Mnp@YM10.

The Raman spectra of Mnp and Mnp@YM10 (see the Online Resource pages 13–14) show a broad strong signal at 663 cm^{-1} and a weaker one around 330 cm^{-1} assigned to phonon modes of magnetite. Peaks at 235, 420, and 1360 cm^{-1} may be associated to the contamination with hematite [37]. However, care should be taken when assigning these species to the original material, since even under 10 mW laser power irradiation and 30 s acquisition time, magnetite undergoes facile laser-induced phase changes to hematite and maghemite phases [21]. YM extract contribution to Mnp@YM10 Raman signals at *ca.* 1100 cm^{-1} (CCO stretching modes of carbonyls) and 1360 cm^{-1} (C–N vibrations) cannot be discarded [17].

Mnp TGA curve (Fig. 2) shows 1.5% mass loss between 120 and 450 °C due to adsorbed ions and phase transformations of the magnetite structure at temperatures of 550–650 °C, in agreement with literature reports [34]. Mnp@YM4 and Mnp@YM10 curves show total mass loss of *ca.* 4 and 10%, respectively, in the temperature range 200 °C < T < 500 °C attributed to the loss of organic matter [34].

The XPS spectra of Mnp and Mnp@YM10 depict the main lines for Fe, O, C, and N. Deconvolution of O1s peaks (see Figure S7 of the Online Resource) of both particles show 75% contribution of a band at 530.0 eV characteristic of O atoms in iron oxide environments [29] and a minor

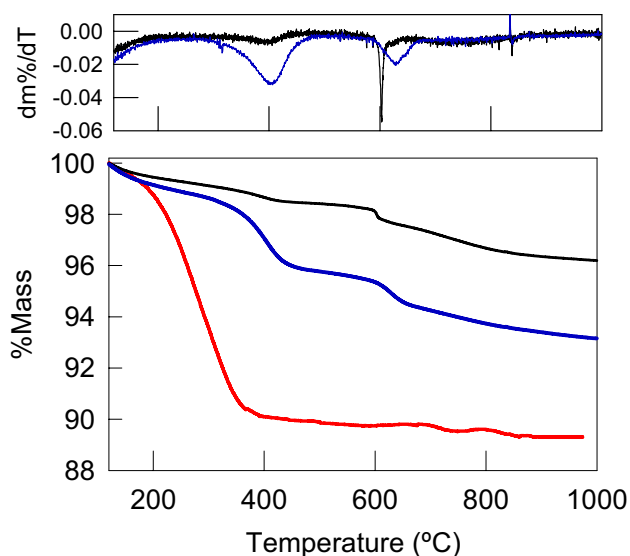


Fig. 2 TGA mass% curves obtained in air atmosphere (bottom figure) and corresponding first derivatives (top figure). Black, blue, and red curves correspond to Mnp, Mnp@YM4, and Mnp@YM10, respectively. (Color figure online)

contribution at 532.8 eV indistinctly attributed to organic oxygen and adsorbed water. Fe2p signals depict Fe2p_{3/2} and Fe2p_{1/2} regions and clear distinguishable satellites (see Figure S8 of the Online Resource). The 2p_{3/2} and 2p_{1/2} peaks and satellite with BE of 711.5, 724.9, and 719.5 eV are characteristic of Fe₂O₃ while those with BE at 710.1, 723.3, and 714 eV are typical of FeO and Fe₃O₄ [43]. Since Mnp and Mnp@YM10 show similar ratio of the 710.1 and 711.5 eV signals area, the contribution of surface Fe(II) and Fe(III) oxides remain independent on the YM coating.

The N1s signals of Mnp and Mnp@YM10 show the contribution of bands at 400.0 and 401.5 eV assigned to organic nitrogen and positively charged nitrogen [29, 36], respectively, as depicted in Fig. 3.

Taking the experimental sensitivity factors relative to the different elements and considering mainly iron oxides contribution to O, approximate surface compositions of Fe₁O_{1.5}N_{0.2} and Fe₁O_{1.4}N₁ are estimated for Mnp and Mnp@YM10, respectively. While both particles show surface oxide composition in line with a mixture of Fe(II) and Fe(III) oxides, a more N-rich coating is observed for Mnp@YM10. C-composition was not analyzed due to adventitious carbon contamination.

The obtained Mnp p*H*_{PZC} = 7.3 is in line with literature reports [20, 39] describing magnetite as an amphoteric surface capable of specifically absorbing H⁺ and OH⁻ leading to Fe-OH₂⁺ and Fe-O⁻ surface charges. Mnp@YM4 and Mnp@YM10 p*H*_{PZC} values are 6.7 and 5.4, respectively. Considering that IR, Raman, and XPS data indicate that phenols, carboxylic acids, and N-H are among the major groups

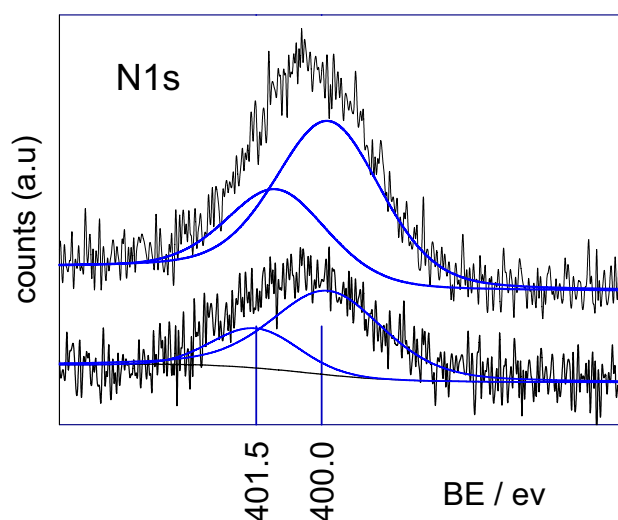


Fig. 3 N1s signals for (from down to top, black curves) Mnp and Mnp@YM10. Blue lines stand for the contributing species proposed from the deconvolution of the signals (see text)

of YM extracts bound to magnetite, YM-coated magnetite might be capable of specifically absorbing H⁺ and OH⁻ leading to NH⁺, O⁻, and COO⁻ surface charged groups causing surface charge reversing at lower pHs.

The average hydrodynamic particle size distribution determined by DLS measurements of Mnp, Mnp@YM4, and Mnp@YM10 in aqueous suspensions are 355 ± 75, 340 ± 60, and 162 ± 5 nm, respectively. These values being several fold-times higher than the individual particle sizes visualized by TEM support the formation of large particle agglomerates in water. The smaller hydrodynamic size observed for Mnp@YM10 agglomerates suggests that these particles form more stable suspensions than Mnp@YM4 and Mnp; also in agreement with the decreasing ξ potential values of -32 ± 1, -7.5 ± 3, and 4 ± 1 mV observed in aqueous suspensions of pH 7 for Mnp@YM10, Mnp@YM4, and Mnp, respectively.

3.2 Radical Scavenging and Antioxidant Properties

ABTS⁺ radical absorbance is depleted by addition of Mnp@YM10, see Online Resource page 6, following a pseudo first order law kinetics which reflects the low mobility, diffusion, and aggregation of the antioxidant nanoparticles. To obtain radical scavenging activities (RSA%) representing the antioxidant capacity of the particles with independence of kinetics, the time dependent RSA% curve was well fitted to an exponential rise to maximum function, as shown in Fig. 4a *Inset*. Obtained fitting parameters are depicted in Table S1 of the Online Resource.

Figure 4a shows the linear relation between RSA% and the concentration of particles. From the slope of these

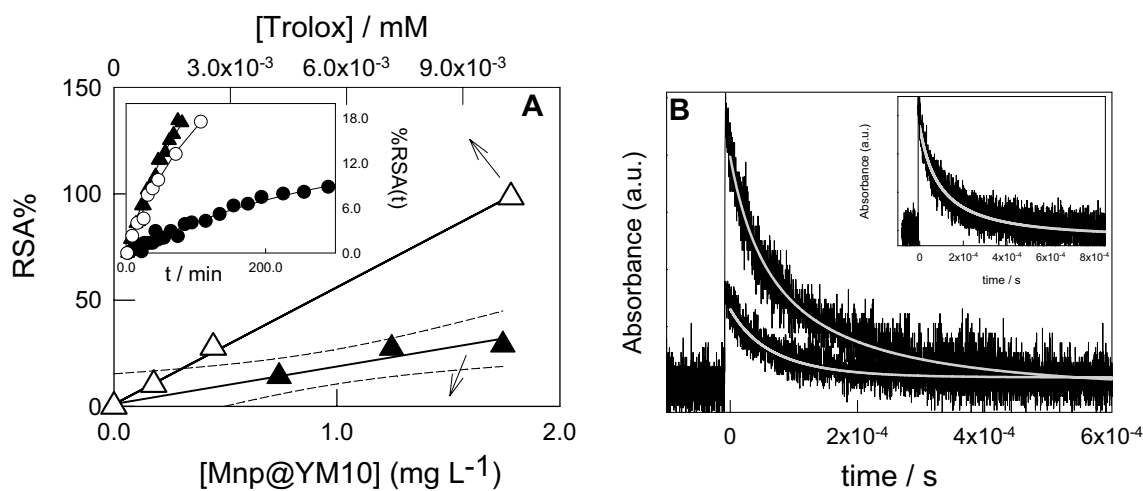


Fig. 4 **a** Dependence of RSA% with the concentrations of Mnp@YM10 (filled triangle) and Trolox (open triangle). *Inset* Evolution of radical scavenging activity, RSA(t)%, with the reaction time for different Mnp@YM10 concentrations: (filled circle) 0.74, (Y) 1.25, and (filled triangle) 1.74 mg L⁻¹. The solid lines stand for the fitting to an

exponential rise to a constant value. **b** SO₄^{•-} radical absorbance traces at 450 nm in suspensions of pH 7, 1.0 × 10⁻² M S₂O₈²⁻ and 0.6 g L⁻¹ of either (from top to down) Mnp and Mnp@YM10. *Inset idem* main figure but in the absence of nanoparticles. Solid grey lines stand for the fitting to a mixed order decay law

lines, RSA% of 17.5 is observed per mg L⁻¹ of Mnp@YM10. The Trolox Equivalent Antioxidant Capacity, TEAC, is of 1.8 μM trolox per mg L⁻¹ Mnp@YM10. Considering that 10% of the particle mass is due to the organic coating and that magnetite itself is not exposed to ABTS^{•+} (*vide infra*), a TEAC of 1.8 μM trolox may be assigned to the scavenging activity of the 0.1 mg YM coating contained in 1 mg particles. Reported values between 180 and 550 μmol trolox/g dried YM extract [41] are well below that found here. However, polyphenols present in YM extract, as epicatechine and quercetin show TEAC values of 1.25 and 2 μM trolox per 0.1 mg L⁻¹, respectively, [32] on the order of the values observed here for YM coatings. Therefore, a high content of polyphenols in Mnp@YM10 is inferred from these experiments.

YM-coating scavenging activity of SO₄^{•-} radical anions was evaluated by analyzing the decay rates of SO₄^{•-} generated by peroxodisulfate anions absorption of a pulse of 266 nm light in the presence and absence of Mnp and Mnp@YM10 (see Online Resource page 8). The kinetic analysis of SO₄^{•-} traces over three half-lives could be well fitted to a simultaneous first and second order decay law (see equation S3 of the Online Resource) as shown in Fig. 4b, in agreement with the well-known reactions of SO₄^{•-} [33]. The reaction rate constant for the second order process is in line with that reported for the bimolecular recombination of SO₄^{•-} radicals, while the first order component, *k*_{app}, corresponds to the reactions of the radical with peroxodisulfate anions (of identical concentration in all the experiments) and with Mnp or Mnp@YM10. SO₄^{•-} decay in the absence and in the presence of Mnp

and Mnp@YM10 yield *k*_{app} = 2100 ± 500, 2200 ± 300, and 11,200 ± 900 s⁻¹, respectively.

Identical *k*_{app} values observed in the absence of nanoparticles and presence of Mnp indicates that the reaction rate constant of Mnp with SO₄^{•-} is < 200 g⁻¹ L s⁻¹. Also, the reaction between Mnp dissolved Fe²⁺ and SO₄^{•-} (*k*(Fe²⁺ + SO₄^{•-}) = 4.6 × 10⁹ M⁻¹ s⁻¹ [8]) does not contribute to SO₄^{•-} decay. Thus, [Fe²⁺] < 0.05 μM in the presence of 1.0 × 10⁻² M S₂O₈²⁻ is estimated. On the other hand, a rough estimation of the absolute rate constant for the reaction between Mnp@YM10 and SO₄^{•-} radicals taking the difference in *k*_{app} values in the presence and absence of 0.6 g L⁻¹ Mnp@YM10 yields *k*_{SO₄^{•-}-Mnp@YM} = (1.5 ± 0.5) × 10⁴ g⁻¹ L s⁻¹. It should be noted, as will be discussed later, that particle agglomeration at the concentration used in these experiments may preclude the accessibility of SO₄^{•-} radicals to the particles surfaces inside the agglomerates. Consequently, the obtained *k*_{SO₄^{•-}-Mnp@YM} may be a lower limit to the ideal situation where no agglomerates are formed.

Considering Mnp size, the density of bulk magnetite, and the 10% weight organic coverage, an average mass of 1 × 10⁻¹⁷ g per Mnp@YM10 is obtained (see Online Resource page 16) and used to estimate *k*_{SO₄^{•-}-Mnp@YM} = (9.5 ± 3) × 10¹⁰ M⁻¹ L s⁻¹ per molar concentration of reactants.

An estimation of the diffusion-controlled rate constant between solution SO₄^{•-} radicals and the surface of a spherical particle yields *k*_{SO₄^{•-}-Mnp@YM} ~ 11 × 10¹⁰ M⁻¹ s⁻¹, as described in Online Resource page 16. The coincidence

between predicted and experimental values strongly suggest that the reaction between $\text{SO}_4^{\cdot-}$ radicals and the YM coating is diffusion-controlled and that the distribution of YM reaction sites along the particle surface is homogeneous.

3.3 Application of NPs as Nanoadsorbent

Figure 5a shows that MB adsorption isotherms obtained from adsorption and desorption experiments in aqueous solutions of pH 7 and 25 °C for each particle type are coincident; thus revealing reversible adsorption processes. The one-adsorption site Langmuir model (see Eq. S5 of the Online Resource) fits MB adsorption isotherms with regression coefficients $r^2 \geq 0.975$. The affinity coefficient, K_L , and the maximum adsorption capacity, b , of MB adsorption on Mnp, Mnp@YM4, and Mnp@YM10 are $K_L = 0.53 \pm 0.07$, 0.43 ± 0.07 , $0.38 \pm 0.06 \text{ Lg}^{-1}$ and $b = 12.8 \pm 0.7$, 30 ± 2 , and $50 \pm 2 \text{ mg g}^{-1}$, respectively. While K_L values show a small decreasing trend with the amount of YM contained per gram particle, b values linearly increase with the YM content as depicted in Fig. 5a inset. The similar order of magnitude

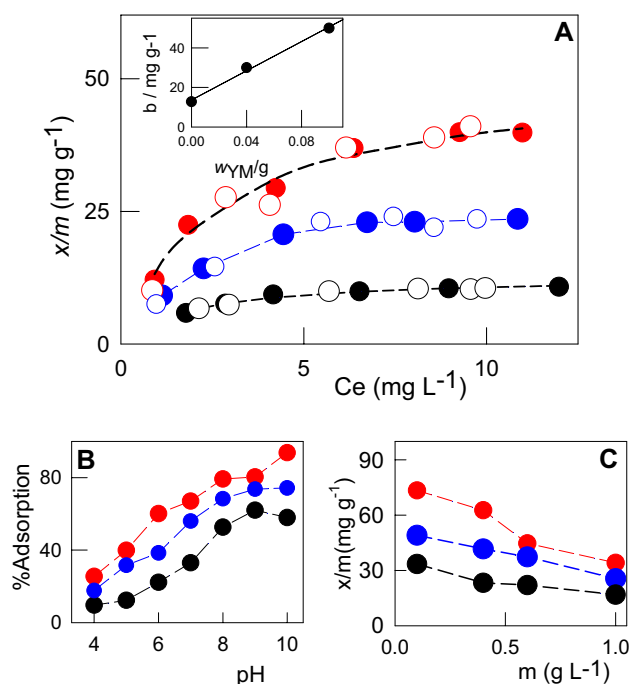


Fig. 5 **a** MB adsorption isotherms in aqueous solutions of pH 7 and 25 °C obtained for experiments with 0.6 gL^{-1} suspensions of either Mnp@YM10, Mnp@YM4, or Mnp. Black, blue, and red symbols stand for Mnp, Mnp@YM4, and Mnp@YM10, respectively. Closed and opened symbols stand for adsorption and desorption experiments, respectively, and lines stand for the fitting of the data to the one-adsorption site Langmuir model. *Inset* Linear dependence of b with the YM content per gram of particle (w_{YM}/g). **b** % adsorption of MB from a 0.6 gL^{-1} nanoparticle suspension of varying pH containing 40 ppm MB. **c** Effect of the particle mass, m , on the removal efficiency per g particle (x/m) of a 40 ppm MB solution at pH 7.0

observed for K_L values might indicate reversible adsorption processes of alike nature, as may be the case for an adsorption mechanism dominated by electrostatic forces. In fact, most reported MB adsorption processes on a variety of different substrates involve electrostatic interactions [1, 2, 6, 28]. Values of b obtained for Mnp@YM10 are in line with those reported for humic acid-coated magnetite nanoparticles [45].

An increase in adsorption with increasing pH is observed for all the particles in the range from 4 to 10, see Fig. 5b, where the adsorption capacity trend $\text{Mnp} < \text{Mnp@YM4} < \text{Mnp@YM10}$ is maintained. Considering that MB remains positively charged (pK_a 3.8) in the pH range studied and that the nanoparticles may become more negatively charged with increasing pH due to the ionization and/or protolytic reactions of YM (COOH and OH) and magnetite (FeOH) surface groups [39], the contribution of electrostatic interactions to the adsorption mechanism is inferred. However, the contribution of specific adsorption, as interaction with surface hydroxyls, at the lower pHs cannot be neglected [28].

For a given initial MB concentration, the removal efficiency per g particle decreases with the increase in the concentration of either Mnp@YM10, Mnp@YM4, and Mnp, as depicted in Fig. 5c. A similar trend is also reported for MB adsorption on natural adsorbents [6]. The observed higher particle agglomeration with increasing suspended mass may be a cause for the reduction of the accessible surface for MB adsorption per gram particle, as suggested for other nanoparticle systems [2, 24]. In fact, agglomerated surface charged colloids may show superposed double layers inducing the diminution of adsorbed surface charges in the internal surfaces between particles [19] thus limiting the available surface sites for adsorption to the external surface of the agglomerates.

3.4 Application of YM-Coated Magnetite Nanoparticles as Oxidation Inhibitor of Adsorbed Substrates

Peroxodisulfate activation, either thermally [26] or by interaction with Fe^{2+} from magnetite [3] is known to produce highly oxidative $\text{SO}_4^{\cdot-}$ radical anions which in turn are capable of initiating MB degradation [14]. In fact, aqueous solutions containing 40 mg L^{-1} MB and $1.0 \times 10^{-2} \text{ M}$ $\text{Na}_2\text{S}_2\text{O}_8$ at 25 °C, either in the absence or presence of 0.6 gL^{-1} of Mnp, showed the diminution of MB concentration in solution, $[\text{MB}]_e$, with the reaction time (see Fig. 6). In the absence of nanoparticles, $[\text{MB}]_e$ diminishes to ca. 24% after 3 h, in agreement with the occurrence of a low efficient $\text{S}_2\text{O}_8^{2-}$ thermal activation [26]. Addition of 6.0 gL^{-1} of Mnp to these solutions causes a faster $[\text{MB}]_e$ diminution reaching ca. 85% after three hours, thus stressing the contribution of

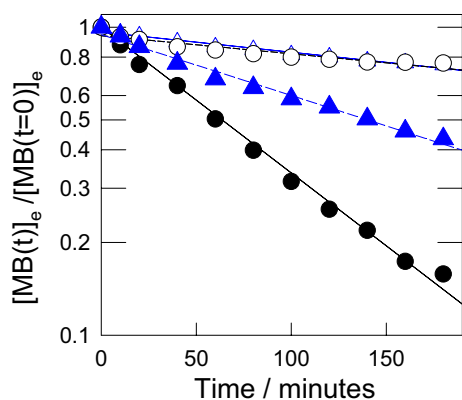


Fig. 6 Semilogarithmic plot of MB solution concentration vs time in 1.0×10^{-2} M $\text{Na}_2\text{S}_2\text{O}_8$ aqueous solutions of pH 7 and 25°C in the absence (open circle) and presence of 0.6 gL^{-1} of either Mnp (filled circle), Mnp@YM4 (filled triangle), and Mnp@YM10 (open triangle)

an efficient magnetite-induced $\text{S}_2\text{O}_8^{-2}$ activation process. Addition of 0.6 gL^{-1} of either Mnp@YM4 or Mnp@YM10 shows $[\text{MB}]_e$ depletion to ca. 56 and 24%, respectively, after 3 h reaction. The latter results strongly support an inhibition effect of YM towards MB degradation when compared to Mnp. The coincident $[\text{MB}]_e$ depletion rates observed for particle-free and Mnp@YM10 experiments suggests that thermal activation of $\text{S}_2\text{O}_8^{-2}$ is the main mechanism taking place in both experiments. Moreover, considering that MB reversibly adsorbs to the particles and assuming that $\text{S}_2\text{O}_8^{-2}$ does not affect the particles adsorption capacity, a total MB concentration taking into account solution and adsorbed MB of ca. 9% after 3 h reaction is estimated for experiments with Mnp@YM10 (see Online Resource page 10). The latter value being smaller than that of particle-free experiments further emphasizes the role of adsorption in the prevention of MB oxidation. Altogether, the obtained results indicate that 10 mg of YM coating per 100 mg magnetite are able to effectively inhibit magnetite $\text{S}_2\text{O}_8^{-2}$ activation due to two main mechanisms: YM efficient $\text{SO}_4^{\cdot-}$ radical scavenging activity and/or formation of a protective layer isolating the magnetite core from $\text{S}_2\text{O}_8^{-2}$ interactions.

4 Conclusions

YM extract-coated magnetite nanoparticles of 15 nm size were obtained in an environmentally-friendly, low cost, efficient, one-pot synthesis procedure. The particles are composed of a crystalline magnetite core surrounded by a shell of magnetite and Fe_2O_3 oxides forming chelates with YM-components containing carboxylic acid groups and phenols and a high content of organic N. YM-coating is capable of specifically absorbing H^+ and OH^- leading to a higher

content of surface charges than Mnp. As a consequence, particle agglomeration is reduced with increasing YM content and more stable homogeneous aqueous suspensions are formed.

The particles are easy to operate and show radical scavenging abilities and reversible adsorption capacity for positively-charged dyes. Radical-scavenging sites are homogeneously distributed along the particle surface and their trolox equivalent antioxidant capacity compares well with that of YM-polyphenols. These capacities play a role in the nanoparticles use as protective scavengers towards the oxidation of molecules in oxidative media, as observed for methylene blue in $\text{Na}_2\text{S}_2\text{O}_8$ solutions. Possible potential applications of YM-coated magnetite nanoparticles as nanoantioxidants and nanoadsorbents include food process engineering,[10] polymer industry, diesel additive,[22] and waste water treatment, [31] among others.

Acknowledgements DFM thanks Consejo Nacional de Investigaciones Científicas y Técnicas (CONICET, Argentina) for a graduate studentship. MCG and PC are research members of CONICET, LSV is a research member from CICPBA, Argentina.

Funding This study was supported by grant PICT 2012-1795 from ANPCyT.

Compliance with Ethical Standards

Conflict of interest The authors declare that they have no conflict of interest.

References

1. L. Ai et al., Removal of methylene blue from aqueous solution with magnetite loaded multi-wall carbon nanotube: Kinetic, isotherm and mechanism analysis. *J. Hazard. Mater.* **198**, 282–290 (2011)
2. O.A. Attallah et al., Removal of cationic and anionic dyes from aqueous solution with magnetite/pectin and magnetite/silica/pectin hybrid nanocomposites: kinetic, isotherm and mechanism analysis. *RSC Adv.*, **6**(14), 11461–11480 (2016). <https://doi.org/10.1039/C5RA23452B>
3. P. Avetta et al., Activation of persulfate by irradiated magnetite: implications for the degradation of phenol under heterogeneous photo-fenton-like conditions. *Environ. Sci. Technol.* **49**(2), 1043–1050 (2015)
4. W.J. Barreto, S. Regina, G. Barreto, Iron oxide and pyrocatechol: a spectroscopy study of the reaction products. *Quim. Nov* **29**(6), 1255–1258 (2006)
5. D.H.M. Bastos et al., Phenolic antioxidants identified by ESI-MS from yerba maté (*Ilex paraguariensis*) and green tea (*Camellia sinensis*) extracts. *Molecules* **12**(3), 423–432 (2007)
6. K.G. Bhattacharya, A. Sharma, Kinetics and thermodynamics of methylene blue adsorption on Neem (*Azadirachta indica*) leaf powder. *Dyes Pigm.* **65**(1), 51–59 (2005)
7. L. Bravo, L. Goya, E. Lecumberri, LC/MS characterization of phenolic constituents of mate (*Ilex paraguariensis*, St. Hil.) and

- its antioxidant activity compared to commonly consumed beverages. *Food Res. Int.* **40**(3), 393–405 (2007)
8. G.V. Buxton, T.N. Malone, & G.A. Salmon. Reaction of SO_4^{4-} with Fe^{2+} , Mn^{2+} and Cu^{2+} in aqueous solution. *J. Chem. Soc. Faraday Trans.* **93**(16), 2893–2897 (1997). <https://doi.org/10.1039/A701472D>
 9. W. Cai, J. Wan, Facile synthesis of superparamagnetic magnetite nanoparticles in liquid polyols. *J. Colloid Interface Sci.* **305**, 366–370 (2007)
 10. Q. Chaudhry, R. Watkins, L. Castle, Nanotechnologies in the food arena: new opportunities, new questions, new concerns. in *Nanotechnologies in Food*, ed. by Q. Chaudhry, C. Laurence, R. Qasim (Springer, Berlin, 2010), pp. 1–17
 11. E.D. Cömert, V. Gökmen, Antioxidants bound to an insoluble food matrix: their analysis, regeneration behavior, and physiological importance. *Compr. Rev. Food Sci. Food Saf.* (2017). <https://doi.org/10.1111/1541-4337.12263>
 12. R.M. Cornell & U. Schwertmann, *The Iron Oxides. Structure, Properties, Reactions, Occurrences and Uses*. 2nd edn. (Wiley-VCH Verlag, Weinheim, 2003). Available at <http://scholar.google.com/scholar?hl=en&btnG=Search&q=intitle:Iron+Oxides+in+the+Laboratory#3>
 13. S.E. Favela-Camacho et al., Stability of magnetite nanoparticles with different coatings in a simulated blood plasma. *J. Nanoparticle Res.* **18**(7), 176 (2016). <https://doi.org/10.1007/s11051-016-3482-2>
 14. A. Ghauch et al., Methylene blue discoloration by heated persulfate in aqueous solution. *Chem. Eng. J.* **213**, 259–271 (2012)
 15. P.R. Ginimuge, Methylene Blue **26**(4), 517–520 (2017)
 16. X.H. Guan, C. Shang, G.H. Chen, ATR-FTIR investigation of the role of phenolic groups in the interaction of some NOM model compounds with aluminum hydroxide. *Chemosphere* **65**(11), 2074–2081 (2006)
 17. S. Gunasekaran, G. Sankari, S. Ponnusamy, Vibrational spectral investigation on xanthine and its derivatives—Theophylline, caffeine and theobromine. *Spectrochimica Acta* **61**(1–2), 117–127 (2005)
 18. C.I. Heck, E.G. De Mejia, Yerba mate tea (*Ilex paraguariensis*): a comprehensive review on chemistry, health implications, and technological considerations. *J. Food Sci.* **72**(9), (2007)
 19. P.C. Hiemenz, R. Rajagopalan, *Principles of Colloid and Surface Chemistry*, 3rd Edn. (CRC Press, New York, 1997). Available at <https://www.crcpress.com/Principles-of-Colloid-and-Surface-Chemistry-Third-Edition-Revised-and-Hiemenz-Rajagopalan/9780824793975#googlePreviewContainer>
 20. J.-D. Hu et al., Effect of dissolved organic matter on the stability of magnetite nanoparticles under different pH and ionic strength conditions. *Sci. Total Environ.* **408**(16), 3477–3489 (2010). Available at <https://www.scopus.com/inward/record.uri?eid=2-s2.0-77953703572&partnerID=40&md5=020aac6b78f74e159a17a96cfc1b6d99>
 21. A.M. Jubb, H.C. Allen, Vibrational spectroscopic characterization of hematite, maghemite, and magnetite thin films produced by vapor deposition. *ACS Appl. Mater. Interfaces* **2**(10), 2804–2812 (2010)
 22. H. Jung, D.B. Kittelson, M.R. Zachariah, The influence of a cerium additive on ultrafine diesel particle emissions and kinetics of oxidation. *Combust. Flame* **142**(3), 276–288 (2005)
 23. G. Magnacca et al., Novel magnetite nanoparticles coated with waste-sourced biobased substances as sustainable and renewable adsorbing materials. *ACS Sustain. Chem. Eng.* **2**(6), 1518–1524 (2014). <https://doi.org/10.1021/sc500213j>
 24. D.F. Mercado Castro et al., Paramagnetic iron-doped hydroxyapatite nanoparticles with improved metal sorption properties. A bioorganic substrates-mediated synthesis. *ACS Appl. Mater. Interfaces* **6**, 3937–3946 (2014)
 25. D.F. Mercado Castro, M.C. Gonzalez, F.H. Sánchez, Yerba Mate applications: magnetic response of powders and colloids of magnetite nanoparticles coated with *Ilex Paraguariensis* derivatives. (2017) (**under review**)
 26. V.C. Mora et al., Thermally activated peroxydisulfate in the presence of additives: a clean method for the degradation of pollutants. *Chemosphere* **75**(10), 1405–1409 (2009)
 27. H. Muthukumar, M. Matheswaran, Amaranthus spinosus leaf extract mediated FeO nanoparticles: physicochemical traits, photocatalytic and antioxidant activity. *ACS Sustain. Chem. Eng.* **3**(12), 3149–3156 (2015)
 28. T.S. Natarajan, H.C. Bajaj, R.J. Tayade, Preferential adsorption behavior of methylene blue dye onto surface hydroxyl group enriched TiO_2 nanotube and its photocatalytic regeneration. *J. Colloid Interface Sci.* **433**, 104–114 (2014). <https://doi.org/10.1016/j.jcis.2014.07.019>
 29. Nist, *NIST X-ray Photoelectron Spectroscopy Database, Version 4.1* (National Institute of Standards and Technology, Gaithersburg, 2012), <http://srdata.nist.gov/xps/>
 30. M. Rafatullah et al., Adsorption of methylene blue on low-cost adsorbents: a review. *J. Hazard. Mater.* **177**(1–3), 70–80 (2010). <https://doi.org/10.1016/j.jhazmat.2009.12.047>
 31. M. Rafatullah et al., Adsorption of methylene blue on low-cost adsorbents: a review. *J. Hazard. Mater.* **177**(1–3), 70–80 (2010)
 32. C. Rice-Evans et al., The relative antioxidant activities of plant-derived polyphenolic flavonoids. *Free Radic. Res.* **22**(4), 375–383 (1995)
 33. J.A. Rosso et al., Reaction of sulfate and phosphate radicals with α,α,α -trifluorotoluene. *J. Chem. Soc. Perkin Trans.* **2**, 205–210 (1999)
 34. M. Rudolph, J. Erler, U.A. Peuker, A TGA-FTIR perspective of fatty acid adsorbed on magnetite nanoparticles-Decomposition steps and magnetite reduction. *Colloids Surf. A* **397**, 16–23 (2012)
 35. S.P. Schwaminger et al., Oxidation of magnetite nanoparticles: impact on surface and crystal properties. *CrystEngComm* **19**(2), 246–255 (2017). Available at <http://xlink.rsc.org/?DOI=C6CE02421A>
 36. C. Socaci et al., Developing novel strategies for the functionalization of core-shell magnetic nanoparticles with folic acid derivatives. *Mater. Chem. Phys.* **162**, 131–139 (2015). Available at <https://doi.org/10.1016/j.matchemphys.2015.05.046>
 37. K. Song et al., Comprehensive design of carbon-encapsulated Fe_3O_4 nanocrystals and their lithium storage properties. *Nanotechnology* **23**(50), 505401 (2012). Available at <http://www.ncbi.nlm.nih.gov/pubmed/23186940>
 38. C. Su, Environmental implications and applications of engineered nanoscale magnetite and its hybrid nanocomposites: a review of recent literature. *J. Hazard. Mater.* **322**, 48–84 (2017). Available at <http://www.sciencedirect.com/science/article/pii/S030438941630615X>
 39. E. Tombácz et al., Magnetite in aqueous medium: coating its surface and surface coated with it. *Rom. Rep. Phys.* **58**(3), 281–286 (2006)
 40. S. Trifunski et al., Determination of flavonoid and polyphenol compounds in *Viscum album* and *Allium Sativum* extracts. *Int. Curr. Pharm. J.* **4**, 382–385 (2015)
 41. M.A. Vieira et al., Phenolic acids and methylxanthines composition and antioxidant properties of mate (*Ilex paraguariensis*) residue. *J. Food Sci.* **75**(3), 280–285 (2010)
 42. L.S. Villata et al., One-electron oxidation of antioxidants : a kinetic-thermodynamic correlation. *Redox Rep.* **18**(5), 205–209 (2013). Available at <http://hdl.handle.net/11336/5237>
 43. T. Yamashita, P. Hayes, Analysis of XPS spectra of Fe^{2+} and Fe^{3+} ions in oxide materials. *Appl. Surf. Sci.* **254**(8), 2441–2449 (2008)

44. L. Zhang, R. He, H.C. Gu, Oleic acid coating on the monodisperse magnetite nanoparticles. *Appl. Surf. Sci.* **253**(5), 2611–2617 (2006)
45. X. Zhang et al., Adsorption of methylene blue onto humic acid-coated Fe_3O_4 nanoparticles. *Colloids Surf. A* **435**, 85–90 (2013)

Affiliations

D. Fabio Mercado¹ · Paula Caregnato¹ · Laura S. Villata¹ · Mónica C. Gonzalez¹

¹ Instituto de Investigaciones Fisicoquímicas Teóricas y Aplicadas (INIFTA), CCT-La Plata-CONICET, Universidad Nacional de La Plata, La Plata, Argentina